

Article

# CFD Modeling of the Catalyst Oil Slurry Hydrodynamics in a High Pressure and Temperature as Potential for Biomass Liquefaction

Artur Wodołański <sup>1</sup>, Jacek Skiba <sup>2</sup>, Katarzyna Zarębska <sup>3</sup>, Jarosław Polański <sup>4</sup> and Adam Smolinski <sup>5,\*</sup> 

<sup>1</sup> Department of Energy Saving and Air Protection, Central Mining Institute, 40-166 Katowice, Poland; awodolazski@gig.eu

<sup>2</sup> Experimental Mine Barbara, Central Mining Institute, 40-166 Katowice, Poland; jskiba@gig.eu

<sup>3</sup> Department of Energy and Fuels, AGH University of Science and Technology, 30-059 Krakow, Poland; katarzyna.zarebska@agh.edu.pl

<sup>4</sup> Institute of Chemistry, Faculty of Science and Technology, University of Silesia in Katowice, 40-006 Katowice, Poland; jpolanski@us.edu.pl

<sup>5</sup> Central Mining Institute, 40-166 Katowice, Poland

\* Correspondence: smolin@gig.katowice.pl; Tel.: +48-32259-2252

Received: 24 September 2020; Accepted: 29 October 2020; Published: 30 October 2020



**Abstract:** The paper presents the simulation of a catalyst-paraffin oil slurry hydrodynamics under high pressure and temperature in a convex bottom reactor with a Rushton turbine which was conducted with an application of computational fluid dynamics (CFD) modeling. An analysis to obtain a uniform distribution of solid catalyst particles suspended in paraffin oil was carried out as a potential for biomass liquefaction. The effects of the particle diameter, bed density, liquid viscosity, and the initial solid loading on slurry hydrodynamics in high pressure and temperature behavior were investigated using the Eulerian–Eulerian two-fluid model and the standard  $k-\epsilon$  turbulence model. The main objective was to assess the performance in agitating highly concentrated slurries to obtain slurry velocity, concentration, the degree of homogeneity, and to examine their effect on the mixing quality. The results of the analysis are applied to predicting the impact of the most efficient conditions on slurry suspension qualities as potential for biomass liquefaction.

**Keywords:** hydrodynamics; CFD modeling; particle suspension; stirred tank reactor

## 1. Introduction

Stirred tank reactors with solid catalyst particles dispersed in a liquid are widely used in chemical industry processes such as the methanol [1,2], Fischer–Tropsch syntheses, or the oxidation of p-xylene to terephthalic acid [3,4]. Their recent use also enables the liquefaction of biomass. One implementation of liquefaction is for the conversion of wet biomass at 573–623 K and 15–18 MPa into oil (biocrude or paraffin). For biomass liquefaction, CuO, ZnO or other catalysts are used [5].

The main advantage of using a stirred-tank reactor is that all particles are dispersed throughout the volume of the slurry reactor, which is a successful elimination of concentration and thermal gradients. This results in a high yield and selectivity of the reaction performed [6]. The main problem associated with mixing is to achieve a homogeneous suspension, which cannot be achieved easily because of complicated solid–liquid multi-physics interactions as well as high-energy dissipation and consumption. Another important issue is the choice of appropriate mixing parameters providing a sufficient degree of catalyst particle fineness in a suspension. One of the most important issues is to

achieve an appropriate contact surface/interface between solid particles and the liquid to provide the desired mass transfer [7,8].

Due to the difficulty to measure solid concentration in regions of high energy dissipation, the slurry hydrodynamics mostly can only be characterized by numerical simulations [7], especially in high pressure and temperature regions, where the use of measuring instruments is impossible.

A mathematical description of the slurry hydrodynamics preparation is difficult due to the interaction between the flow around the rotating agitator and stationary baffle [8]. Achieving an adequate quality suspension is the most important factor in meeting the desired product quality [9,10]. The computational fluid dynamics (CFD) enables for a better understanding of two-phase liquid–solid hydrodynamics, which are reliability and safety, especially under high pressure and temperature conditions. Additionally, visualizing the multiphase flow structure in a stirrer tank supplies precise details of the concentration profile and provides an opportunity to predict suspension quality [3,11]. The modeling of suspension hydrodynamics constitutes an important issue, because it may be applied to explaining the phenomenon of heat and mass transfer in synthesis reactions. The CFD simulation of particle suspension in a stirred tank has been studied by many researchers, for example, Murthy et al. [11], Qi et al. [8], Khopkar et al. [12], Kasat et al. [4], Wodołański [13], and Fradette et al. [14]. However, the hydrodynamics of CuO/ZnO slurry catalyst has not been sufficiently investigated and quantitatively described [15]. The available literature lacks data describing high pressure slurry catalyst behavior in a stirrer tank reactor. However, CFD modeling of slurry (CuO/ZnO particles in paraffin oil) hydrodynamics with two blade impeller in a stirrer tank reactor has been previously conducted [14]. Hydrodynamics associated with the flow of biomass through the catalyst bed will have a great potential for biomass liquefaction in high pressure and temperature.

Agitation energy is an important aspect in the design and operation of a stirred reactor and is dissipated mainly in the shearing and circulation of fluid in the reactor. The power number ( $Np$ ), a dimensionless number describing the power characteristic of the impeller, is often used to reflect the degree of stirring and the motion state of liquid in a reactor.  $Np$  can be correlated mathematically, usually based on experimental data measured under similar geometric conditions with the same type of agitator. The catalyst particles cannot be measured experimentally or controlled during the high-pressure process. The quantities characterizing the catalysis process and its impact on a given chemical reaction are experimentally immeasurable, and the stresses occurring inside the catalytic mechanism under high pressure are inaccessible and impossible for measuring devices due to environmental conditions (high pressure and temperature). Computational fluid dynamics (CFD) has been used extensively to analyse the hydrodynamics or flow field in a stirred reactor. Energy from impeller is highly consumed by liquid circulation and, in high pressure and temperature, has an essential role in hydrodynamic slurry behaviour.

High pressure and temperature conditions can be used in stirrer and tube reactor in technology: for coal/biomass gasification [16,17], methanol or Fischer-Tropsch synthesis, and other waste-to-energy conversion, such as biomass hydrothermal liquefaction or bio-oil production. Biomass liquefaction demands thermochemical conversion (high temperature and pressure) to transform lignocelluloses biomass into energy or fuels. Co-gasification of coal and biomass [18] in clean coal technologies plays an important role in the energy transformation, which has recently become a significant potential in the production of hydrogen as an environment friendly energy carrier. The share of this carrier will play an increasingly important role, where the technology of its acquisition will depend on modern methods of liquefying biomass into liquid fuels, but it requires more energy-costly technologies due to the use of high pressure and temperature. The catalyst used under these conditions may also have a limited service life and often requires regeneration [19]. The type of raw material subjected to liquefaction also plays an important role. The improving quality of product in biomass liquefaction also depends on zirconia composition studied by Osada and Watanabe [20]. It was found that zirconia raises the conversion efficiency of some products from biomass liquefaction.

The above simulation studies show that the study of the hydrodynamics of the catalyst for biomass liquefaction under high pressure and temperature conditions will play an increasingly important role in the optimization of the biomass liquefaction process in the future, which can have a significant impact on the process performance.

In the current work, a three-dimensional CFD model of a stirrer tank reactor with a convex bottom was to be developed for a two-phase high-pressure liquid–solid system. The hydrodynamics of the catalyst for biomass liquefaction was examined, the physicochemical properties of which were taken from a publication [14].

Thus, the main objective of this study was to examine the influence of high pressure and temperature in the tank reactor on the process of different concentration particle suspension, slurry homogeneity, and its mixing quality catalyst using in biomass liquefaction. The process of biomass liquefaction itself was not considered in this article and is a stage of future research.

Simulation studies have demonstrated a significant effect of pressure and temperature on the catalyst suspension behavior. Moreover, it was examined how different operating conditions such as solid loading, particle size, and the impeller speed determine the velocity and concentration fields of a suspension. The results will be applied in future research studies on the efficient processing of biogas/synthesis gas conversion from coal/biomass gasification/liquefaction to methanol/dimethylether in a three-phase system. In the present study, the attention mainly focused on evaluating the feasibility and effectiveness of bio-energy production, which potential is in behavior of the heterogeneous catalyst CuO/ZnO.

## 2. Materials and Method

The three-dimensional CFD model with Eulerian–Eulerian approach was employed to compute the hydrodynamics of a solid–liquid phase in a stirred tank with Rushton turbine. Each of the phases, liquid and solid, was treated as a continuum interacting with each another. The governing equations are given below:

Continuity equation:

$$\frac{\partial(\alpha_i \rho_i)}{\partial t} + \nabla \cdot (\alpha_i \rho_i \vec{u}_i) = 0 \quad (1)$$

Momentum equation:

$$\frac{\partial(\alpha_i \rho_i \vec{u}_i)}{\partial t} + \nabla \cdot (\alpha_i \rho_i \vec{u}_i \vec{u}_i) = -\alpha_i \nabla p_i + \nabla \cdot \left( \alpha_i \mu_i \left( \nabla \vec{u}_i + (\nabla \vec{u}_i)^T \right) \right) + \vec{F}_C + \vec{F}_i + \alpha_i \rho_i \vec{g} \quad (2)$$

where:  $\alpha_i$  is volume fraction,  $\rho_i$  is density,  $\vec{u}_i$  is velocity,  $\vec{F}_C$  is centrifugal and Coriolis forces,  $\vec{F}_i$  is total interfacial force, and  $p_i$  is pressure.

The standard k– $\epsilon$  turbulence model for the liquid phase describing the kinetic energy of turbulence  $k$  and its dissipation  $\epsilon$  is described as:

$$\frac{\partial}{\partial t} (\alpha_l \rho_l \vec{u}_l) + \nabla \cdot (\alpha_l \rho_l \vec{u}_l k_l) = \nabla \cdot \left[ \alpha_l \left( \mu_l + \frac{\mu_{tl}}{\sigma_k} \right) \nabla k_l \right] + \alpha_l P_l - \alpha_l \rho_l \epsilon_l \quad (3)$$

$$\frac{\partial}{\partial t} (\alpha_l \rho_l \epsilon_l) + \nabla \cdot (\alpha_l \rho_l \vec{u}_l \epsilon_l) = \nabla \cdot \left[ \alpha_l \left( \mu_l + \frac{\mu_{tl}}{\sigma_\epsilon} \right) \nabla \epsilon_l \right] + \alpha_l \frac{\epsilon_l}{k_l} (C_{\epsilon 1} \rho_l - C_{\epsilon 2} \rho_l \epsilon_l) \quad (4)$$

where:  $\epsilon$  is turbulence dissipation rate, and  $\mu_{tl}$  is viscosity for liquid.

Parameters in the standard k– $\epsilon$  model and the following values are selected as follows:  $C_{\epsilon 1} = 1.45$ ,  $C_{\epsilon 2} = 1.9$ ,  $\sigma_k = 1.0$ , and  $\sigma_\epsilon = 1.3$ . The values of these constants were obtained by means of numerous iterations of data fitting for a wide range of turbulent flows [12,15,21].

The mixture turbulence model assumes the domain as a mixture and solves for  $k$  and  $\varepsilon$  values which are common for both phases. The drag component of the solid–liquid interfacial force is given by [22]:

$$\vec{F}_{is}^D = \frac{3}{4} \frac{C_{D,is}}{d_s} \rho_l \alpha_s |\vec{u}_s - \vec{u}_l| (\vec{u}_s - \vec{u}_l) \quad (5)$$

where drag coefficient  $C_{D,is}$  exerted by the solid–liquid phase is obtained by means of the Schiller Naumann drag model [23]:

$$C_{D,is} = \max\left(\frac{24}{\text{Re}} (1 + 0.15 \text{Re}^{0.687}), 0.44\right) \quad (6)$$

where the Re number is:

$$\text{Re} = \frac{\rho_l d_s |\vec{u}_s - \vec{u}_l|}{\mu} \quad (7)$$

where  $\mu$  is viscosity, and  $\vec{u}_{s,l}$  is the velocity for solid–liquid phase

The liquid phase turbulent viscosity is calculated using the Sato enhanced turbulence model (Sato, 1998):

$$\mu_{tl} = C_{\mu} \rho_l \frac{k^2}{\varepsilon} + C_{\mu,p} \rho_l \alpha_s d_s |\vec{u}_s - \vec{u}_l| \quad (8)$$

where  $\mu_{tl}$  is the conventional shear-induced turbulent viscosity:

$$\mu_{tl} = C_{\mu} \rho_l \frac{k^2}{\varepsilon} \quad (9)$$

Solid turbulent viscosity is proportional to the liquid phase  $\mu_{tl}$  [15]:

$$\mu_{ts} = \frac{\rho_s}{\rho_l} \frac{\mu_{tl}}{\sigma_t} \quad (10)$$

where  $\sigma_t$  is a turbulent Prandtl number appropriate to the solid phase kinematic eddy viscosity  $\mu_{ts}$ . Turbulent Prandtl number for slurry was 1.42.

The homogeneous distribution of solids [24] in stirred reactors is often very important in the operation and design of a stirred reactor. Full homogeneous solid suspension in a liquid is usually impossible to achieve owing to the unevenness of the flow field in the reactor. Equation (9) using the standard deviation of the solid concentration to evaluate the degree of suspension gives:

$$\sigma = \sqrt{\left[ \sum_{i=1}^n (\alpha_{si} / \alpha_{s,avg} - 1)^2 / n \right]} \quad (11)$$

where:  $n$  is the number of sampling locations for measuring the local holdup of solid phase,  $\alpha_{si}$  is the solid volume fraction of the sampling location, and  $\alpha_{s,avg}$  is the average solid volume fraction in the reactor.

The lower the standard deviation  $\sigma$ , the better the suspension quality. The standard deviations of the paraffin oil–solid particle system are based on the simulated data using the  $\alpha_{si}$  stored in all the computational cells. Simulated deviations of solid suspension are also quite consistent with mesh.

A stirred tank reactor with Rushton turbine was the subject of the modeling. Figure 1 shows the stirred tank reactor geometry and mesh. The selected reactor and impeller dimensions are shown in Table 1. The dimensions are in accordance with the design guidelines for a six-bladed Rushton turbine (RT) impeller disc located at a distance of 0.1 m from the reactor bottom. Figure 2 shows a schematic diagram of the RT impeller-driven stirred tank with dimensions, marked on the drawing.

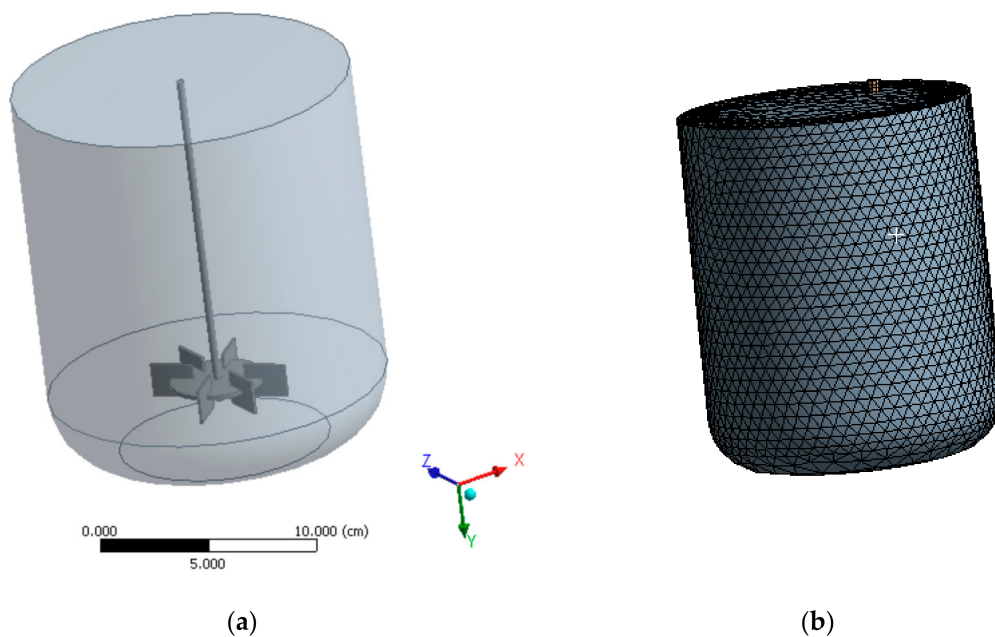


**Figure 1.** Geometry of a convex bottom reactor (a), and mesh of a convex bottom reactor (b).

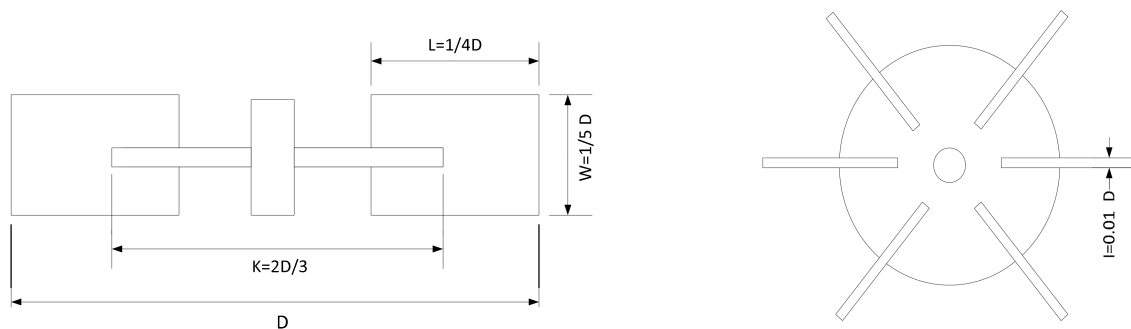


**Figure 2.** Schematic diagram of the Rushton turbine (RT) impeller-driven stirred tank.

The preliminary computations were performed for three meshes with different densities to check the mesh independence and improve the consistency and accuracy of the calculation model. In order to solve the problem of the interface between the moving and stationary zones, the two approaches of multiple reference frame (MRF) model and sliding mesh model were applied. In the CFD simulation of flow field, the number of grid nodes usually has an influence on the solid distribution and mixing process.

Grid-independent results are fine enough for 53,000 cells. The mesh parameters for simulation (max angular skewness 0.76, minimum orthogonal quality of cells 0.21, and maximum aspect ratio 11.12) have been checked for appropriate quality. The simulated solid distribution contour plots based on three different grid sizes showed no considerable difference.

The Courant–Friedrichse–Lewy (CFL) criterion for the numerical stability for the time step size 0.001 s was 0.51. Influence of flow fields to the grid sizes sensitive on the simulated solid distribution was also checked. Unsteady state simulations under various operating conditions were carried out using Fluent. As the node-based averaging scheme is more accurate than the default cell based scheme for triangular and tetrahedral meshes, the Green–Gauss Node-based method was adopted for computing the gradient and standard wall functions were used for the simulation. The absolute convergence criterion was specified as the residual value of 0.001.

All terms of the governing equations were discretized using the first order upwind scheme in the simulation, while the SIMPLE algorithm was used for the pressure–velocity coupling. The computational time step was set to be 0.001s with 50 internal iterations.

**Table 1.** Selected reactor and impeller dimensions.

Parameter	Value
Height (m)	0.72
Reactor diameter (m)	0.30
Blades height (m)	0.02
Blades width (m)	0.025
The width of the hub (m)	0.07
The width of the impeller (m)	0.10

A user defined function (UDF) in FLUENT has been applied to coordinate impeller Reynolds number. The steady state was achieved considering the homogeneous distribution of the catalyst particles. The basic numerical control parameters are presented in Table 2.

**Table 2.** Numerical control parameters.

Spatial Discretization	
Gradient	Green-Gauss Node Based
Pressure	Body Force Weighted
Momentum	SIMPLE
Volume Fraction	SIMPLE
Transient formulation	First Order Implicit
Under-Relaxation Factor	
Pressure	0.5
Density	0.8
Momentum	0.4
Slip Velocity	0.1
Volume fraction	0.8

The simulation was carried out to predict the hydrodynamic slurry behavior in the range of high pressures of 50–350 bar and temperatures of 523–753 K. The physical properties of the liquid and solid particles are provided in Table 3. The simulation was run for about 50 s with time step size 0.01 s. The paraffin oil was considered as a continuous phase, whereas catalyst particles were considered as a dispersed phase.

**Table 3.** Parameters of numerical simulation for catalyst particle properties in solid–liquid system.

Parameter	Value
Mixer power (W)	4.5–7.3
The rotational speed of the stirrer (rpm)	300–800
The density of the catalyst bed ( $\text{kg}/\text{m}^3$ )	800–2900
Pressure (MPa)	5–35
The amount of paraffin oil (mL)	150
The size of the catalyst particles ( $\mu\text{m}$ )	100; 300
Catalyst loading (weight %)	0–20

### 3. Results and Discussion

Unsteady state numerical simulations of a slurry hydrodynamics using the commercially available CFD software of Fluent 12.0 were carried out for different particle densities and liquid viscosities. Several computations were carried out to mainly predict the solid concentration of slurry hydrodynamics

profiles. Figure 3 shows axial profiles of particle solid concentrations ( $\alpha_s = 11.0$  vol.%,  $d_s = 100$   $\mu\text{m}$ ) of a stirred tank at times from 0 s to 50 s. The highest concentration of particulates for a given period of time is changing due to the dynamic character of slurry behavior. Slurry is kept as a sticky body that rises up in the first seconds and then breaks down into smaller particles after about 40 s. At time 50 s, a uniform suspension concentration in the entire reactor volume was observed.

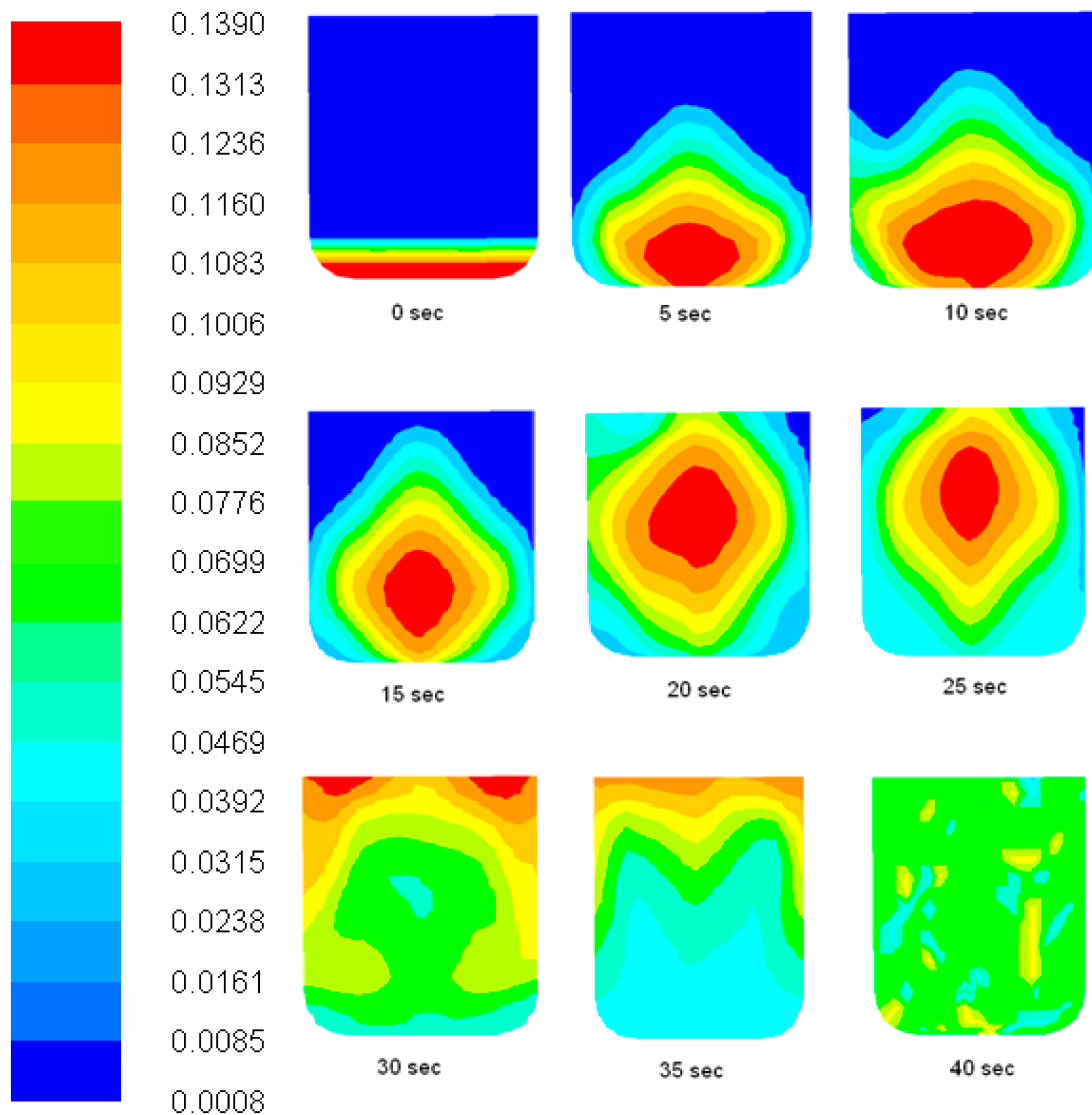


**Figure 3.** Profiles of slurry distribution contour plots under different times at 5-s intervals from 0 s to 40 s, (impeller rotor per minute 300,  $p = 100$  bar, temperature = 673 K).

As shown in Figure 3, the simulation showed that, under high pressure, the suspension becomes a higher viscosity and leads to a homogenous suspension, thus reducing interaction between particles and liquid, which disintegrates after about 50 s. In order to distribute the suspension evenly (catalyst particles in paraffin oil), an appropriate rotational speed of the stirrer was required. The increase in temperature, in turn, caused homogeneous mixture separating into an aggregated particle suspension with a large degree of heterogeneity of particle velocities and concentrations.

Figure 4 demonstrates the sample flow pattern of velocity vectors of 11.0 vol.% of catalyst solid particles of liquid paraffin oil. It can be observed how slurry concentration was distributed for different time intervals from 20 s to 40 s. Slurry flow field was turbulent. Additionally, an interaction between

slurry two phases, i.e., solid particles and paraffin oil, can be seen. Simultaneously, the effects of pressure, temperature, and impeller speed were investigated.

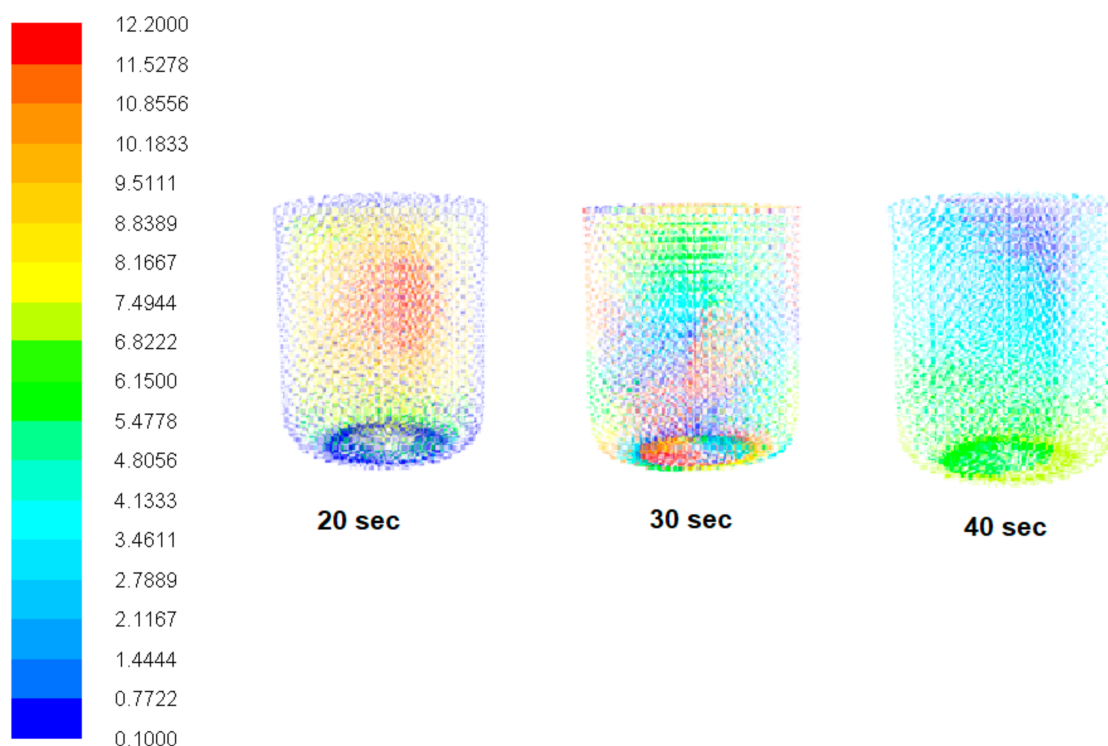


**Figure 4.** Solid velocity vector profiles (m/s) in stirred tank under different times at 10-s intervals from 20 s to 40 s (impeller rotor per minute 300,  $p = 50$  bar, temperature = 695 K).

Figure 5a shows slurry concentration profiles at 100 bar and 700 K throughout the entire reactor domain. The distribution of solid catalyst particles for initial loading was 38 vol.%. Figure 5b shows the path lines of solid catalyst particles. Figure 5 demonstrates that the solids accumulate at the outer surface of the suspension. Tangential velocity induced particle separation due to centrifugal force generated by the impeller rotational speed on suspends. This phenomenon plays an important role in the catalytic reaction where the reagent has an access to the catalyst surface, especially in biomass liquefaction. Figure 5c presents the path lines for the high shear mixer of slurry behavior in 20 s.

With the increase in the impeller speed, a change of hydrodynamics of solid particle distribution may be observed. It can be helpful to reduce the particle accumulation at the mixer bottom. The shape of the reactor bottom not only prevents the accumulation of solids' particles, but also improves the rise of the particulates to the top of the mixer. The characteristic swirl pattern occurs in the mixing zone. Based on the simulation results shown in Figures 3 and 4, it may be concluded that the hydrodynamics of the slurry in the reactor depends mainly on the stirrer rotational speed, physicochemical properties of the slurry, and loading of the solid phase in suspension. The presence of slurry region lowers the mixing overall efficiency and may produce stationary solid particle deposits on the bottom of the reactor. The solid particles move in the liquid phase, and the interaction forces are produced, which include lift force, virtual mass force, and drag force.

In this system, the density of the solid phases is far greater than that of the liquid phase, and the virtual mass force is much smaller than the drag force. The homogeneous suspension of solid catalyst particles mainly depended on mixer power and solid phase density.

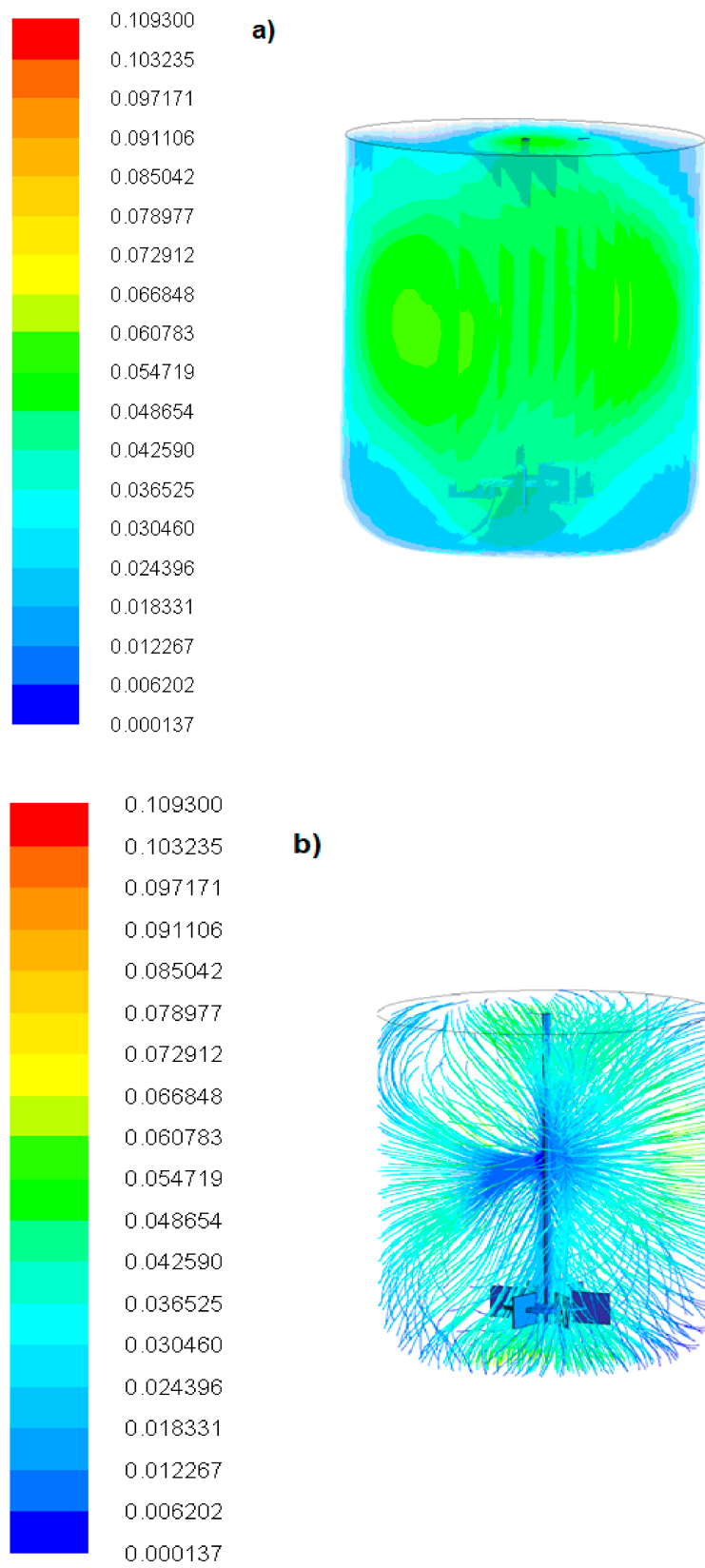
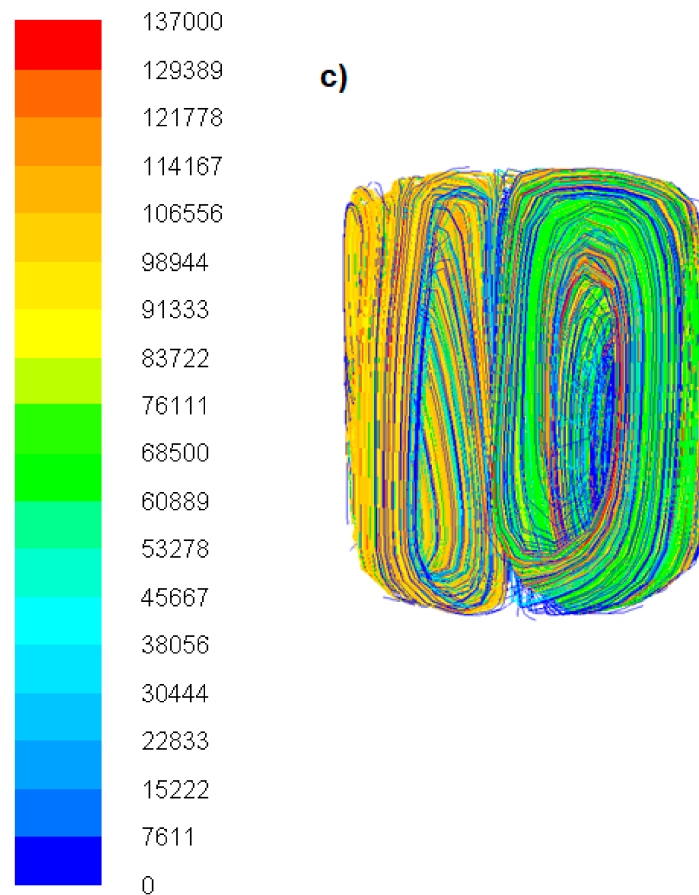
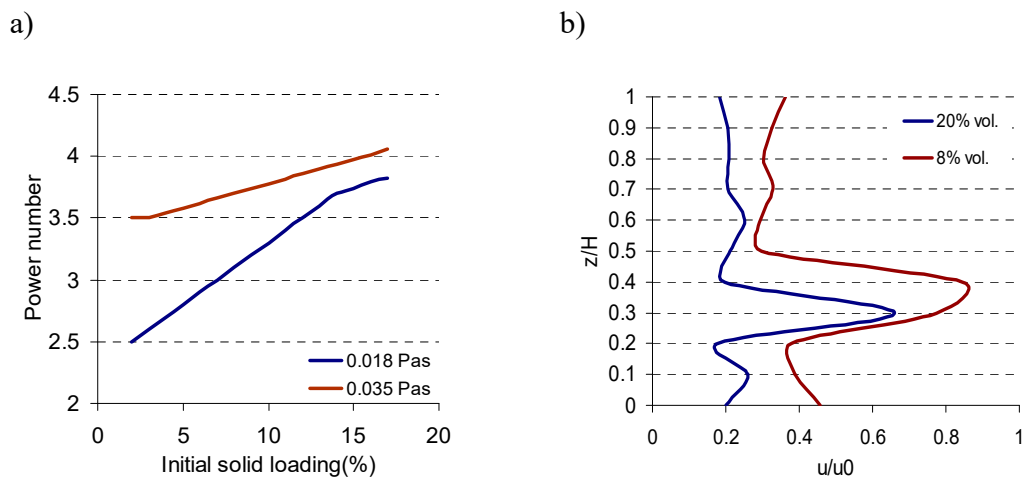


Figure 5. Cont.



**Figure 5.** (a) Slurry (solid and liquid) concentration profiles in stirred tank; (b) Path lines of solid particles; (c) Hydrodynamics path lines of suspension  $d_s = 300 \mu\text{m}$ . Operating conditions: 100 bar, 700 K, impeller rotor per minute: 800.

In order to understand the effect of solid concentration on slurry behavior under high pressure condition, the impacts of stirrer speed, initial solid loading, as well as particle diameter and bed density on slurry hydrodynamics have been examined. Figure 6a demonstrates that increasing the loading of solid catalyst particles requires much more mixing power. The slurry viscosity also affects the amount of power consumed by the impeller. More homogeneous solid particle distribution is obtained in a more viscous liquid. Figure 6b shows the distribution profiles of the axial velocity component of the suspension at different loadings of the solid phase. The volume of solid phase loading (8%) was maintained for a much longer time. Increase of the initial solid loading from 8 to 20 vol.% causes the axial liquid velocity distribution decreases.



**Figure 6.** (a) Mixing power for different values of slurry viscosity ( $\mu = 0.018, 0.035$  Pas) at various solid loadings (2–18%) for  $d_s = 100 \mu\text{m}$ ; (b) Axial velocity distribution of the liquid at selected loadings of solid particles ( $\alpha = 8\%; 20\%$  vol.).

Figure 7 shows normalized solid concentration for different sizes of the catalyst particles and various bed densities. The uniformity of solid particles increases and depends on catalyst particle size. At a time of about 50 s and stirrer speed of 300 rpm, the dispersed particles collected from the bottom of the tank are uniformly suspended.

The holdup of catalyst particles below the impeller was larger than that above the impeller, and the maximum local holdup of catalyst particles in the reactor appeared under the impeller at the tank bottom. Depending on various operating conditions, the homogeneity of the slurry is achieved faster with the increase in impeller rotation speed and the decrease in the loading of the solid phase. A higher catalyst particle density or larger particle size causes faster settling velocity (due to gravity settling) and less homogenous distribution of the particles. Increasing the bulk density of the catalyst slurry leads to a reduction of the homogeneity of particle suspension.

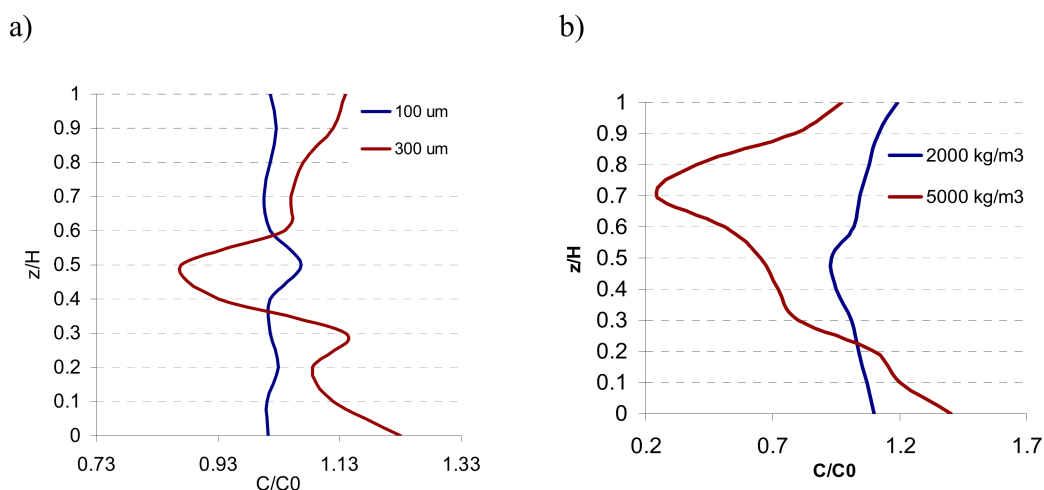


**Figure 7.** Normalized solid concentration for different values of (a) the catalyst particle size ( $d_s = 100 \mu\text{m}, 300 \mu\text{m}$ ) and (b) bed densities ( $\rho = 2000, 5000 \text{ kg/m}^3$ ) for dimensionless axial coordinate  $z/H$ .

#### 4. Conclusions

The CFD three-dimensional hydrodynamic model of slurry catalyst in a stirred tank reactor with six-blade Rushton turbine was developed. Based on the Ansys Fluent numerical simulation, the influence of impeller rotational speed on slurry dispersion degree in a liquid–solid system

was considered. The flow pattern and particle suspension characteristics in a stirred tank were presented. The hydrodynamic analyses of the biomass liquefaction catalyst have a significant influence on the process factors that are due to higher porosity; biochar will play a vital role and will serve as an economical source. This has a significant impact on the economy of the entire process. Numerical analysis showed how the catalyst for the liquefaction of biomass behaves with the increase in viscosity. The extent of slurry suspension improved significantly with an increase in impeller speed; more vortices were also observed, greatly affecting the circulation in the tank.

The hydrodynamics of the catalyst has a significant influence on the biomass liquefaction; in the future, experimental research will be carried out. Hydrodynamics and quality of slurry suspension is of the greatest importance for the stirrer reactor design and control. Solid velocity appeared near the vertical axis of the tank below the impeller, which is attributable to the accumulation of solid particles at the reactor bottom. Higher initial solid loadings contributed to a non-uniform solid distribution in a less viscous liquid. Based on the standard deviations, good solid suspensions could be achieved at impeller speeds of 473 rpm.

Increase of the numerical grid density has significantly longer simulation time, but this allows to precise designation of mixing intensity zones. Factors which affect the suspension of solid particles play an important role in heterogeneous syntheses such as biomass liquefaction or dimethyl ether (DME) synthesis. In high pressure and temperature operating conditions, the CFD simulations of slurry hydrodynamics can be extremely useful for predicting catalyst concentration throughout the whole reactor volume. The model developed can be applied to predicting the accumulation of solid suspension as well as to optimizing the reactor design in order to achieve the optimal slurry concentrations in the entire reactor volume for biomass liquefaction. Furthermore, the simulation results presented will be applied in future studies to build a three-phase system for biomass liquefaction and DME synthesis.

**Author Contributions:** Conceptualization, A.W., A.S., K.Z., J.P., and J.S.; methodology, A.W., A.S., J.S., J.P., and K.Z.; formal analysis, A.W., K.Z., J.P., and A.S.; investigation, A.W. and J.S.; writing—original draft preparation, A.W.; writing—review and editing, A.W.; visualization, A.W.; supervision, A.S. All authors have read and agreed to the published version of the manuscript.

**Funding:** This research received no external funding.

**Acknowledgments:** In this section you can acknowledge any support given which is not covered by the author contribution or funding sections. This may include administrative and technical support, or donations in kind (e.g., materials used for experiments).

**Conflicts of Interest:** The authors declare no conflict of interest.

## References

1. Wodołański, A. Numerical modelling of methanol synthesis. Part 1. Process analysis in a two- and three-phase industrial system Modelowanie numeryczne procesu syntezy metanolu. Cz. I. Analiza przebiegu procesu w układach dwu- i trójfazowym w skali przemysłowej. *PRZEMYSŁ CHEMICZNY* **2015**, *1*, 103–107. [[CrossRef](#)]
2. Wodołański, A. Numerical modelling of methanol synthesis. Part 2. CFD simulation in a three-phase slurry reactor Modelowanie numeryczne procesu syntezy metanolu. Cz. II. Symulacja CFD procesu w trójfazowym reaktorze zawieszinowym. *PRZEMYSŁ CHEMICZNY* **2015**, *1*, 206–212. [[CrossRef](#)]
3. Hosseini, S.; Patel, D.; Ein-Mozaffari, F.; Mehrvar, M. Study of Solid–Liquid Mixing in Agitated Tanks through Computational Fluid Dynamics Modeling. *Ind. Eng. Chem. Res.* **2010**, *49*, 4426–4435. [[CrossRef](#)]
4. Kasat, G.R.; Khopkar, A.R.; Ranade, V.V.; Pandit, A.B. CFD simulation of liquid-phase mixing in solid–liquid stirred reactor. *Chem. Eng. Sci.* **2008**, *63*, 3877–3885. [[CrossRef](#)]
5. Leng, L.; Leng, S.; Chen, J.; Yuan, X.; Li, J.; Li, K.; Wang, Y.; Zhou, W. The migration and transformation behavior of heavy metals during co-liquefaction of municipal sewage sludge and lignocellulosic biomass. *Bioresour. Technol.* **2018**, *259*, 156–163. [[CrossRef](#)]
6. Magelli, F. Modelling of solids distribution in stirred tanks: analysis of simulation strategies and comparison with experimental data. *Int. J. Comput. Fluid Dyn.* **2005**, *19*, 253–262. [[CrossRef](#)]
7. Ochieng, A.; Lewis, A.E. CFD simulation of solids off-bottom suspension and cloud height. *Hydrometallurgy* **2006**, *82*, 1–12. [[CrossRef](#)]

8. Qi, N.; Wu, G.; Wang, H.; Zhang, K.; Zhang, H. CFD simulation of mixing characteristics in stirred tank by Smith turbine. *J. Chem. Ind. Eng.* **2010**, *61*, 2305–2313.
9. Sivashanmugam, P.; Prabhakaran, S. Simulation of an Effect of a Baffle Length on the Power Consumption in an Agitated Vessel. *Int. J. Food Eng.* **2008**, *4*, 1–16. [[CrossRef](#)]
10. Qi, N.; Wang, H.; Zhang, K.; Hu, Z. Numerical simulation of fluid dynamics in the stirred tank by the SSG Reynolds Stress Model. *Front. Chem. Eng. China* **2010**, *4*, 506–514. [[CrossRef](#)]
11. Murthy, B.; Ghadge, R.; Joshi, J. CFD simulations of gas–liquid–solid stirred reactor: Prediction of critical impeller speed for solid suspension. *Chem. Eng. Sci.* **2007**, *62*, 7184–7195. [[CrossRef](#)]
12. Khopkar, A.R.; Kasat, G.R.; Pandit, A.A.B.; Ranade, V.V. Computational Fluid Dynamics Simulation of the Solid Suspension in a Stirred Slurry Reactor. *Ind. Eng. Chem. Res.* **2006**, *45*, 4416–4428. [[CrossRef](#)]
13. Wodołażski, A. Modelling of slurry hydrodynamics with two-blade impeller in tank reactor. *Maint. Reliab.* **2014**, *16*, 533–536.
14. Fradette, L.; Tanguy, P.A.; Bertrand, F.; Thibault, F.; Ritz, J.-B.; Giraud, E. CFD phenomenological model of solid–liquid mixing in stirred vessels. *Comput. Chem. Eng.* **2007**, *31*, 334–345. [[CrossRef](#)]
15. Yamazaki, H.; Tojo, K.; Miyanami, K. Concentration profiles of solids suspended in a stirred tank. *Powder Technol.* **1986**, *48*, 205–216. [[CrossRef](#)]
16. Wodołażski, A.; Smoliński, A. Modelling and process integration study of dimethyl ether synthesis from syngas derived from biomass gasification: Flowsheet simulation. *Alex. Eng. J.* **2020**, *8*, 1. [[CrossRef](#)]
17. Smoliński, A.; Stańczyk, K.; Kapusta, K.; Howaniec, N. Analysis of the organic contaminants in the condensate produced in the in situ underground coal gasification process. *Water Sci. Technol.* **2013**, *67*, 644–650. [[CrossRef](#)]
18. Howaniec, N.; Smoliński, A. Effect of fuel blend composition on the efficiency of hydrogen-rich gas production in co-gasification of coal and biomass. *Fuel* **2014**, *128*, 442–450. [[CrossRef](#)]
19. Chen, Y.; Dong, L.; Miao, J.; Wang, J.; Zhu, C.; Xu, Y.; Chen, G.; Liu, J. Hydrothermal liquefaction of corn straw with mixed catalysts for the production of bio-oil and aromatic compounds. *Bioresour. Technol.* **2019**, *294*, 122148. [[CrossRef](#)]
20. Osada, M.; Sato, T.; Watanabe, M.; Shirai, M.; Arai, K. CATALYTIC GASIFICATION OF WOOD BIOMASS IN SUBCRITICAL AND SUPERCRITICAL WATER. *Combust. Sci. Technol.* **2006**, *178*, 537–552. [[CrossRef](#)]
21. Chapman, C.; Nienow, A.; Cooke, M.; Middleton, J. Particle-gas-liquid mixing in stirred vessels. Part I: particle–liquid mixing. *Chem. Eng. Res. Des.* **1983**, *61*, 71–81.
22. Rewatkar, V.B.; Rao, K.S.M.S.R.; Joshi, J.B. Critical impeller speed for solid suspension in mechanically agitated three-phase reactors. 1. Experimental part. *Ind. Eng. Chem. Res.* **1991**, *30*, 1770–1784. [[CrossRef](#)]
23. Bernstein, W.Z. *Deutsch. Leb. Sprachen* **1987**, *32*, 318–320. [[CrossRef](#)]
24. Bartrand, T.A.; Farouk, B.; Haas, C.N. Countercurrent gas/liquid flow and mixing: Implications for water disinfection. *Int. J. Multiph. Flow* **2009**, *35*, 171–184. [[CrossRef](#)]

**Publisher’s Note:** MDPI stays neutral with regard to jurisdictional claims in published maps and institutional affiliations.



© 2020 by the authors. Licensee MDPI, Basel, Switzerland. This article is an open access article distributed under the terms and conditions of the Creative Commons Attribution (CC BY) license (<http://creativecommons.org/licenses/by/4.0/>).